Electronic Supplementary Material (ESI) for Journal of Materials Chemistry A.

Supporting Information for

Reinforcing the Stability of Cobalt-free Lithium-rich Layered Oxides via Li-poor Ni-rich Surface Transformation

Experimental section

Material preparation

$Li_{1.2}Mn_{0.6}Ni_{0.2}O_2$ (LMNO) cathode materials were prepared by co-precipitation method. Firstly, the required molar amounts of nickel acetate tetrahydrate ($(CH_3COO)_2Ni \cdot 4H_2O$) and manganese acetate tetrahydrate ($(CH_3COO)_2Mn \cdot 4H_2O$) were weighed according to the chemical formulas of the LMNO cathode materials, which were dissolved in a mixed solvent of 150 ml of deionized water and 150 ml of anhydrous ethanol to formulate a transition metal solution; Next, oxalic acid powder with a molar ratio of 1:2 with nickel acetate tetrahydrate and manganese acetate tetrahydrate was weighed and dissolved in 150 ml of anhydrous ethanol to formulate an oxalic acid solution. Subsequently, the configured transition metal solution was poured into the separatory funnel, and the oxalic acid solution was placed on a magnetic stirrer with a heating table for constant temperature stirring at 80 ℃, and the drip rate of the separatory funnel was controlled to be 3-4 ml min^{-1} to drop into the oxalic acid solution to obtain the precursor. The fully precipitated precursor was washed after filtration to remove excess oxalic acid from the surface. Subsequently, the required molar amount (5% excess) of lithium hydroxide was weighed and ground with the resulting precursor to make a homogeneous mixture. The fully precipitated precursor was washed after filtration to remove excess oxalic acid from the surface. Subsequently, the required molar amount (5% excess) of lithium hydroxide was weighed and ground with the resulting precursor to make a homogeneous mixture. The resulting mixture was placed in a muffle furnace and heated to 450 ℃ at a rate of 5 ℃ min^{-1} for 6 h. Subsequently, the same heating rate was taken to 850 ℃, 900 ℃, and 950 ℃ for 12 h to obtain unmodified LMNO samples and excessive calcination treated LMNO samples. The three groups of samples are denoted as $LMNO_{850}$, $LMNO_{900}$, and $LMNO_{950}$.

Material characterization

In this thesis, the crystal structure of the samples was characterized using SmartLab type Rational-Turning Target XRD with a step scan of 0.02° at 10° per

minute over a range of 10-80°. Scanning electron microscope (SEM) type SU-70 was used to analyze the morphology of the Li-Mn-rich cathode material before and after modification. A JEOL ARM200F transmission electron microscope (TEM) was used to characterize the morphology, lattice striations, and selected area electron diffraction of the Lithium-rich manganese cathode material before and after modification. The materials are analyzed for composition using an energy spectrometer (EDS), the model used in conjunction with a scanning electron microscope and a transmission electron microscope. The chemical state of the surface elements is analyzed using an X-ray photoelectron diffraction analyzer, type S4-Explorer. Thermogravimetric analysis of the prepared samples was carried out using a thermogravimetric analyzer (TGA) type TGA-Q50. The chemical compositions of the materials and the after cycling electrolyte were measured by inductively coupled plasma-atomic emission spectrometry (ICP-AES, iCAP 7400).

Electrochemical characterization

Firstly, the binder polyvinylidene fluoride (PVDF) was dissolved using the organic solvent N-methylpyrrolidone (NMP) to make a 3 wt% solution, and then the cathode material, conductive carbon black and binder were mixed uniformly according to the mass ratio = 8:1:1 and then quickly mixed using a defoamer to obtain the cathode slurry. The cathode slurry was placed on the aluminum foil and evenly coated on the aluminum foil by an automatic coating machine.

After coating, the aluminum foil was dried at 80 ℃ in a blast drying oven until the organic solvent evaporated completely, and then transferred to a vacuum drying oven at 120 ℃ for 12 hours. The aluminum foils were punched into cathode electrodes with a diameter of 10 mm by means of a manual punching machine. The active substance was calculated by comparing the mass ratio of coated and blank aluminum foils and with conductive carbon black and binder.

The coin cell assembly was carried out in a glove box in an argon atmosphere with water and oxygen values not exceeding 0.01 ppm. The battery case was a model 2032 coin cell case, the separator was a Celgard 2350 composite diaphragm, the electrolyte was a lithium-ion cathode electrolyte of 1 M $LiPF_6$ (EC:DEC = 1:1, v/v), the cathode electrode was laboratory-prepared, and the anode electrode was a commercially available Li chip. The assembled coin cell is placed on the sealing machine to complete the sealing, and then electrochemical testing is carried out after the electrolyte is fully

infiltrated with the active material.

In this work, the CT3001A model battery test system was used to test the battery performance of the prepared coin cell batteries in the voltage range of 2.0-4.8V. The results such as specific capacity-voltage curve and cycles-specific capacity curve were obtained by constant-current charge/discharge test, and the information of initial capacity, initial Coulombic efficiency, average discharge voltage, cycle stability, and rate performance of the half-cells were thus obtained.

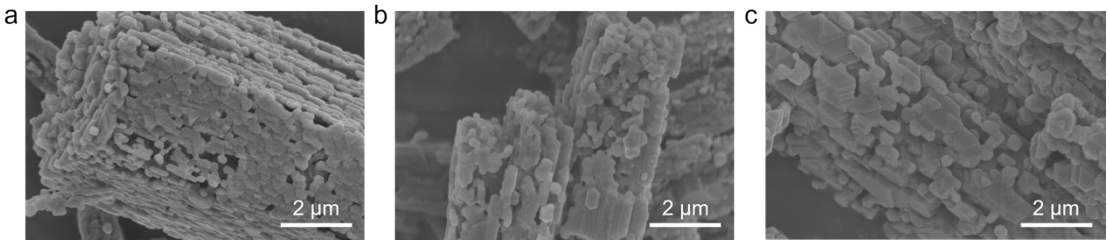

Fig. S1. (a-c) Enlarged images of SEM of (a) $LMNO_{850}$, (b) $LMNO_{900}$, and (c) $LMNO_{950}$ samples.

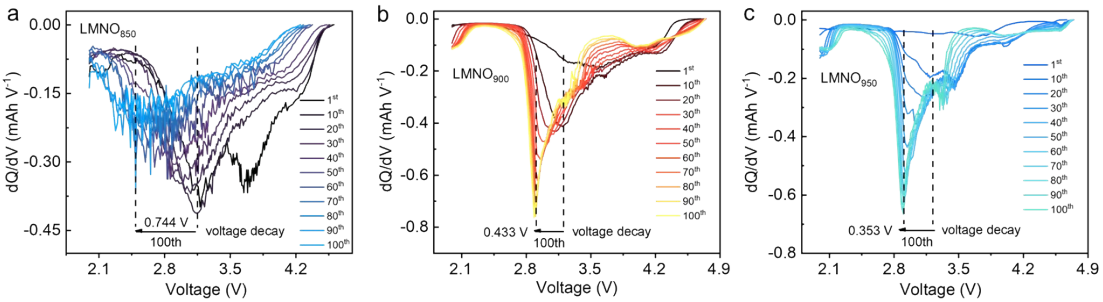

Fig. S2. Corresponding dQ/dV curves for the discharge process of (a) $LMNO_{850}$, (b) $LMNO_{900}$, and (c) $LMNO_{950}$ samples.

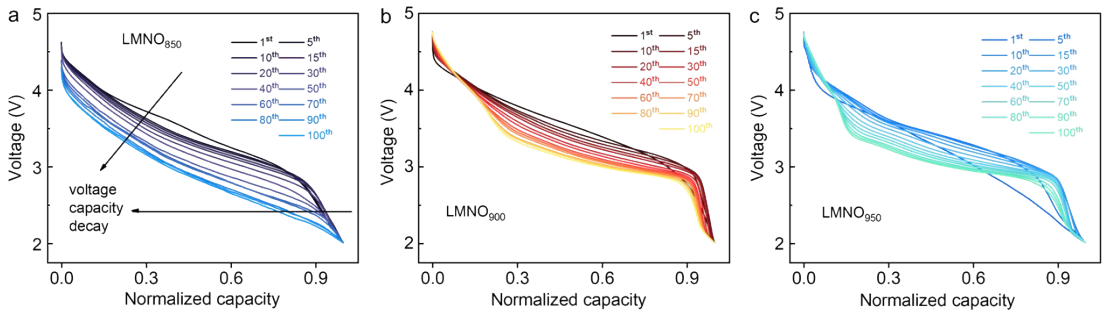

Fig. S3. Normalized voltage curves during discharge of (a) $LMNO_{850}$, (b) $LMNO_{900}$, and (c) $LMNO_{950}$ samples.

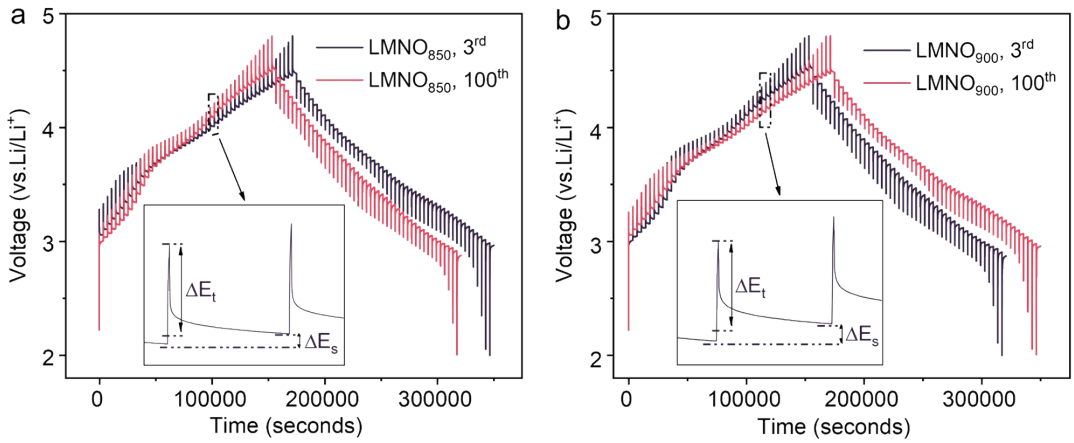

Fig. S4. (a) Galvanostatic intermittent titration technique (GITT) curves of $LMNO_{850}$ and **(b)** $LMNO_{900}$ samples at the 3^{rd} and 100^{th} cycles. The illustration in the figure shows the voltage variation curve, where the change in voltage during constant current charging (discharging) of ΔE_s, ΔE_t is the voltage change caused by a pulse. During the testing process, charge and discharge at a current of 1C for 1 minute each time, and then let it stand for 60 minutes.

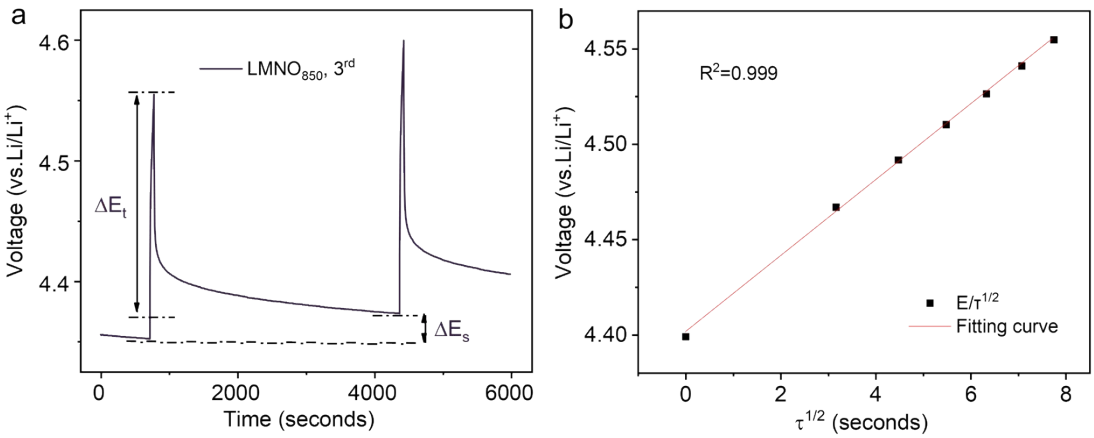

Fig. S5. $LMNO_{850}$ during charging process GITT's (a) schematic diagram of single-step operation and (b) linear relationship between ΔE_t and $\tau^{1/2}$. Fig. S5b was obtained from Fig. S5a, and Fig. S5b was fitted linearly. The fitted linear correlation coefficient, R^2 = 0.999, is close to 1, suggesting that ΔE_t is linearly related to $\tau^{1/2}$.

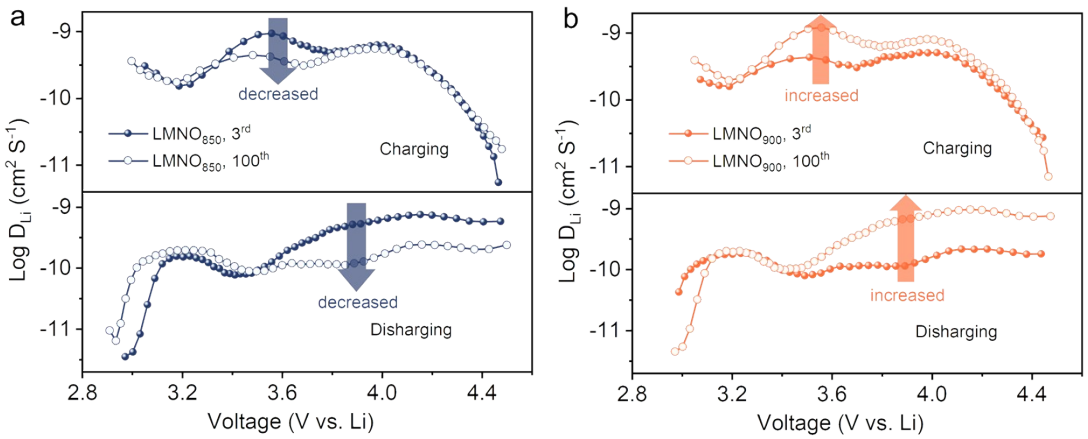

Fig. S6. Li^+ diffusion coefficients of $LMNO_{850}$ and $LMNO_{900}$ samples during the 3rd and 100th cycles. From Fig. S5b, ΔE_t is linearly related to $\tau^{1/2}$. At this point, according to Fick's second law, the diffusion coefficient D_{Li}^+ of Li^+ can be calculated by the following equation:

$$DLi+ = \frac{4}{\pi\tau}\left(\frac{nmVm}{S}\right)2\left(\frac{\Delta Es}{\Delta Et}\right)2$$

In the formula τ—— is the relaxation time;

n_m - is the number of moles;

V_m - is the molar volume of electrode material;

S - is the contact area of the electrode/electrolyte;

$\triangle E_s$ - is the voltage change caused by pulses;

$\triangle E_t$ - is the voltage change during constant current charging (discharging).

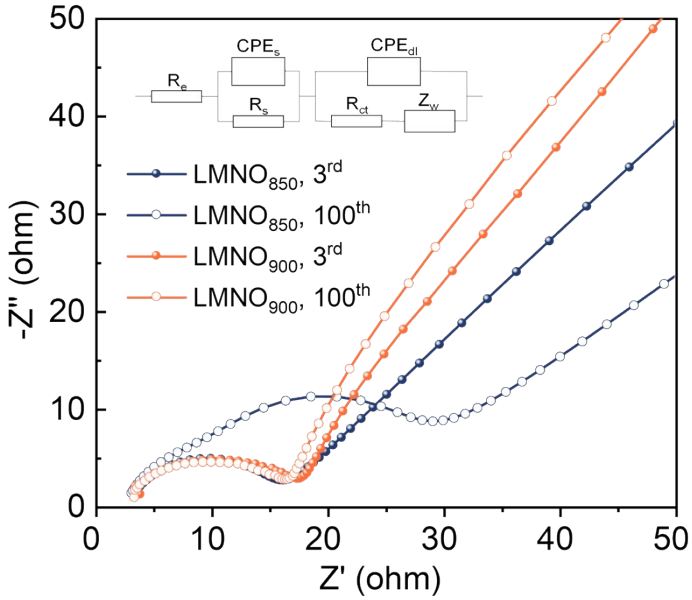

Fig. S7. Electrochemical impedance spectroscopy (EIS) curves of $LMNO_{850}$ and $LMNO_{900}$ samples at the 3rd and 100th cycles. The illustration in the figure shows the equivalent circuit of the EIS curve, where CPE_s and CPE_{dl} are constant phase angle components associated with the SEI layer and double layer, respectively. According to the equivalent circuit fitting of the EIS curve, the R_{ct} of the $LMNO_{850}$ sample during the third cycle was 2.749 Ω, while the R_{ct} of the $LMNO_{900}$ sample was 3.090 Ω. However, after 100 cycles, the R_{ct} of the $LMNO_{850}$ sample increased to 9.592 Ω, while the R_{ct} of the $LMNO_{900}$ sample only increased to 3.601 Ω. Therefore, the $LMNO_{900}$ sample exhibits a more stable charge transfer resistance.

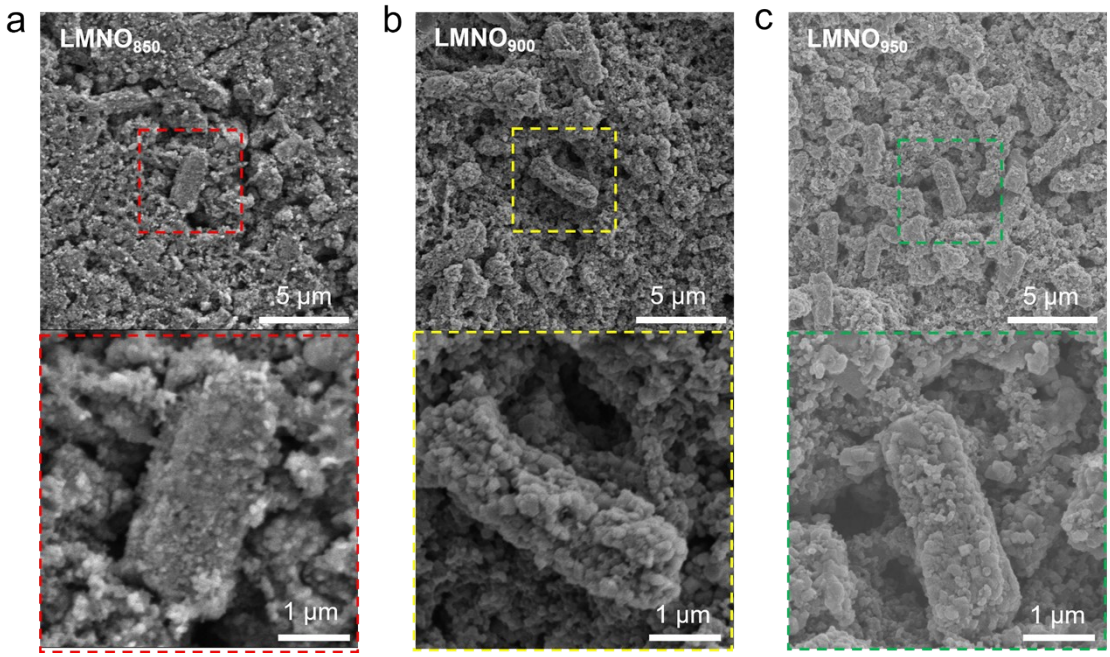

Fig. S8. (a) After cycling 100 cycles SEM image of $LMNO_{850}$ sample and enlarged image of the corresponding rectangular box area. (b) After cycling 100 cycles SEM image of $LMNO_{900}$ sample and enlarged image of the corresponding rectangular box region. (c) After cycling 100 cycles SEM image of $LMNO_{950}$ sample after 100 cycles and magnification of the corresponding rectangular box area.

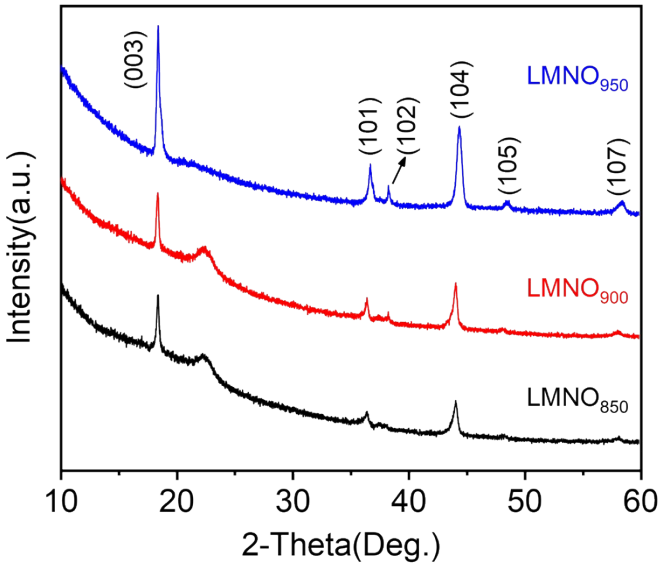

Fig. S9. After cycling 100 cycles XRD patterns of $LMNO_{850}$, $LMNO_{900}$, and $LMNO_{950}$ samples.

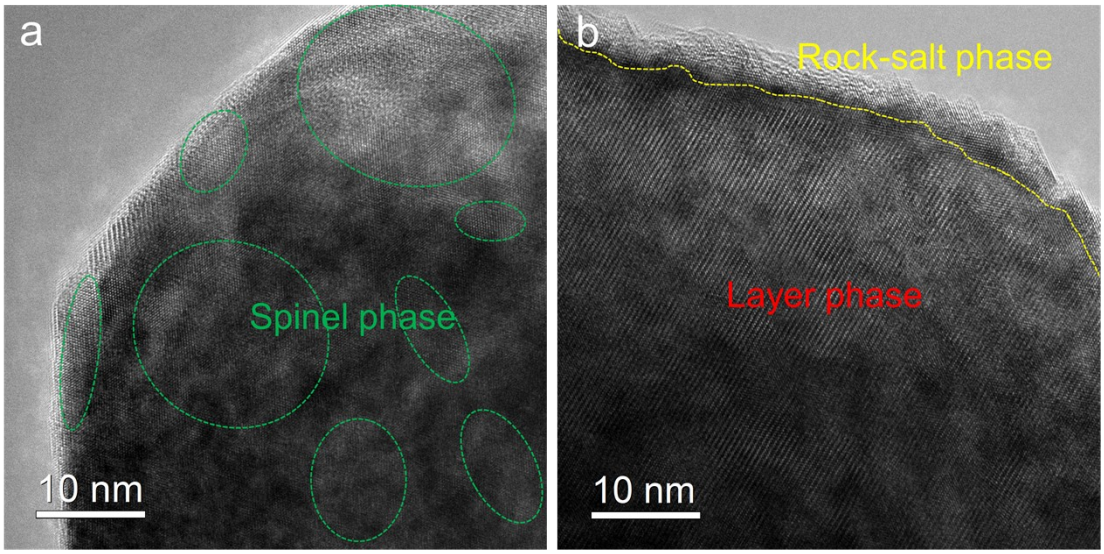

Fig. S10. TEM images of (a) $LMNO_{850}$ and (b) $LMNO_{900}$ samples after 100 cycles

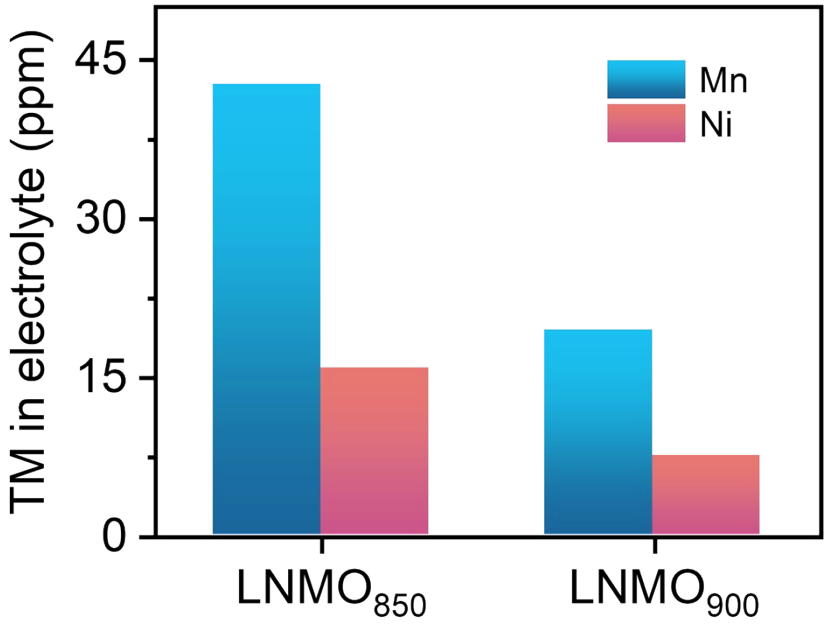

Fig. S11. Dissolved Ni and Mn species in the electrolytes after 100 cycles of the $LMNO_{850}$ and $LMNO_{900}$ samples.

Table S1. Crystallography details of $LMNO_{850}$, $LMNO_{900}$, and $LMNO_{950}$ obtained from joint Rietveld refinement using XRD data.

Sample	$LMNO_{850}$	$LMNO_{900}$	$LMNO_{950}$
$R\bar{3}m$ (%)	50.77	49.33	36.67
C2/m (%)	48.30	46.20	45.52
$Fm\bar{3}m$ (%)	0.23	2.80	13.47
$Fd\bar{3}m$ (%)	0.70	1.67	4.34

Phases Space group	$R\bar{3}m$			C2/m		
Sample	$LMNO_{850}$	$LMNO_{900}$	$LMNO_{950}$	$LMNO_{850}$	$LMNO_{900}$	$LMNO_{950}$
a (Å)	2.8587407	2.8576604	2.8490310	5.0052843	4.9778430	4.9371993
b (Å)	2.8587407	2.8576604	2.8490310	8.5661726	8.5473467	8.5422510
c (Å)	14.2543354	14.2527795	14.2518821	5.0493907	5.0495203	5.0463860
α (°)	90.0000	90.0000	90.0000	90.000	90.000	90.000
β (°)	90.0000	90.0000	90.0000	109.46	109.46	109.46
γ (°)	120.0000	120.0000	120.0000	90.000	90.000	90.000
V ($Å^3$)	100.88512	100.79789	100.18373	204.13071	202.57061	200.67222
R_{wp} (%)	1.596	2.286	2.485	0.679	1.332	1.602

Space ground: $R\bar{3}m$						
Samples	Atom	x	y	z	Wyckoff site	Site occupancy factor
$LMNO_{850}$	Li 1	0	0	0	3a	0.882
	Li 2	0	0	0.5	3b	0.118
	Ni 1	0	0	0	3a	0.118
	Ni 2	0	0	0.5	3b	0.381
	Mn 1	0	0	0.5	3b	0.5
	O 1	0	0	0.24410	6c	1
$LMNO_{900}$	Li 1	0	0	0	3a	0.882
	Li 2	0	0	0.5	3b	0.118
	Ni 1	0	0	0	3a	0.118
	Ni 2	0	0	0.5	3b	0.381
	Mn 1	0	0	0.5	3b	0.5
	O 1	0	0	0.24410	6c	1
$LMNO_{950}$	Li 1	0	0	0	3a	0.882
	Li 2	0	0	0.5	3b	0.118
	Ni 1	0	0	0	3a	0.118
	Ni 2	0	0	0.5	3b	0.381
	Mn 1	0	0	0.5	3b	0.5
	O 1	0	0	0.24410	6c	1

Space ground: $Fm\bar{3}m$						
Samples	Atom	x	y	z	Wyckoff site	Site occupancy factor
$LMNO_{850}$	Li 1	0	0	0	4a	0.2
	Ni 1	0	0	0	4a	0.457
	Ni 2	0	0	0	4a	0.343
	O 1	0.5	0.5	0.5	4b	1
$LMNO_{900}$	Li 1	0	0	0	4a	0.2
	Ni 1	0	0	0	4a	0.457
	Ni 2	0	0	0	4a	0.343
	O 1	0.5	0.5	0.5	4b	1
$LMNO_{950}$	Li 1	0	0	0	4a	0.2
	Ni 1	0	0	0	4a	0.457
	Ni 2	0	0	0	4a	0.343
	O 1	0.5	0.5	0.5	4b	1

Space ground: $Fd\bar{3}m$						
Samples	Atom	x	y	z	Wyckoff site	Site occupancy factor
$LMNO_{850}$	Li 1	0	0	0	8a	1
	Mn 1	0.62500	0.62500	0.62500	16d	1
	Mn 2	0.62500	0.62500	0.62500	16d	1
	O 1	0.38780	0.38780	0.38780	32e	1
$LMNO_{900}$	Li 1	0	0	0	8a	1
	Mn 1	0.62500	0.62500	0.62500	16d	1
	Mn 2	0.62500	0.62500	0.62500	16d	1
	O 1	0.38780	0.38780	0.38780	32e	1
$LMNO_{950}$	Li 1	0	0	0	8a	1
	Mn 1	0.62500	0.62500	0.62500	16d	1
	Mn 2	0.62500	0.62500	0.62500	16d	1
	O 1	0.38780	0.38780	0.38780	32e	1

Table S2. Composition of $LMNO_{850}$, $LMNO_{900}$, and $LMNO_{950}$ samples based on ICP-AES results. Here, the decrease in Li content is attributed excessive calcination treatment leading to the loss of Li, while the increase in Mn and Ni content can be attributed to the increase in $LiMn_2O_4$ phase and $Li_{0.4}Ni_{1.6}O_2$ phase.

Sample	Atomic percent (%)		
	Li	Mn	Ni
$LMNO_{850}$	1.206	0.597	0.197
$LMNO_{900}$	1.169	0.623	0.208
$LMNO_{950}$	1.076	0.692	0.232

Table S3. Discharge specific capacity (mAh g^{-1}) of $LMNO_{850}$, $LMNO_{900}$ and $LMNO_{950}$ samples at different C-rates.

Materials	0.1C	0.2C	0.5C	1C	2C	4C
$LMNO_{850}$	256.0	205.7	155.6	120.1	103.4	10.8
$LMNO_{900}$	225.2	200.5	163.8	125.7	93.8	51.4
$LMNO_{950}$	162.5	142.5	117.5	89.8	62.5	29.3

Table S4. First and 100th discharge medium voltage (V) of $LMNO_{850}$, $LMNO_{900,}$ and $LMNO_{950}$ samples.

Materials	First discharge average voltage	100th discharge average voltage	Discharge average voltage retention rate
$LMNO_{850}$	3.395	2.7965	82.3%
$LMNO_{900}$	3.5224	3.0745	87.3%
$LMNO_{950}$	3.3921	3.0036	88.5%

Table S5. Dissolved Ni and Mn in the electrolytes measured by ICP-OES after 100 cycles under 1C.

Sample	Mn in electrolyte (ppm)	Ni in electrolyte (ppm)
$LMNO_{850}$	42.65	15.80
$LMNO_{900}$	19.38	7.51